

# Quantum optical theory of the quantum-dot Mollow triplet in an exciton-driven semiconductor cavity-QED system

C. Roy\* and S. Hughes†

*Department of Physics, Engineering Physics and Astronomy,  
Queen's University, Kingston, Ontario, Canada K7L 3N6*

We present a comprehensive theoretical study of the resonance fluorescence spectra of an exciton-driven quantum dot (QD) placed inside a high- $Q$  semiconductor cavity and interacting with an acoustic phonon bath. We derive a quantum master equation (ME) in the polaron frame which includes exciton-phonon and exciton-cavity coupling to all orders. This work details and extends the theory used in a recent issue of *Physics Review Letters* (C. Roy and S. Hughes 2011 Phys. Rev. Lett. **106** 247403) to describe the QD Mollow triplet in the regime of semiconductor cavity-QED. Here we introduce two ME forms, Nakajima-Zwanzig (NZ) and time-convolutionless (TC), both to second order in the system-phonon-reservoir perturbation. In the polaron frame, these two ME forms are shown to yield equivalent population dynamics and fluorescence spectra for a continuous wave (cw) driving field. We also demonstrate that a Markov approximation is valid for computing the incoherent scattering rates and we subsequently exploit the Markovian TC ME to explore the resonance fluorescence spectra of an exciton-driven quantum dot. Both cavity-emitted and exciton-emitted spectra are studied and these are found to have quite different spectral features. For the driven quantum-dot-cavity system, the well known characteristics of the atomic Mollow triplet are shown to be considerably modified and we highlight in detail the key effects arising from both cavity coupling and electron-phonon coupling. Regimes of pronounced cavity feeding and anharmonic cavity-QED are exemplified, and we find that the cavity coupling depends sensitively on the QD-cavity detuning and the temperature of the phonon reservoirs. For relatively small exciton-cavity couplings, the full width at half maximum (line width) of the Mollow triplet sidebands varies approximately linearly with the square of the Rabi frequency of the cw pump, which is in good agreement with recent experiments. Phonon-mediated cavity coupling also contributes to the spectral broadening of the Mollow triplet depending upon the detuning and the strength of the exciton-cavity coupling rate. Finally, we investigate the fluorescence spectra for off-resonance cw driving and study the resulting spectral line width of the Mollow triplet sidebands.

PACS numbers: 42.50.Ct, 78.67.Hc, 78.55.-m

## I. INTRODUCTION

Semiconductor quantum dots (QDs) interacting with microcavities are a field of intense research where ideas from conventional cavity-quantum electrodynamics (cavity-QED) have been applied and studied<sup>1,2</sup>. These systems show enormous promise for technological applications ranging from quantum information processing and quantum metrology to the creation of single photon on demand<sup>3-9</sup>. The possibility of exploiting quantum *anharmonicities* in these cavity-QED systems may also lead to photon blockade which is of great interest to generate nonclassical light states<sup>10</sup>. Additionally, the spin degree of freedom of the underlying excitonic states is of interest for quantum information processing<sup>11</sup>. In the past few years, an increasing number of experimental studies have focussed on resonance fluorescence of a QD coupled to a cavity mode<sup>12-15</sup>. Progress has also been made in the study of off-resonant QD cavity system that can be used to observe the photoluminescence (PL) spectra of the QD or the cavity<sup>16-18</sup>.

Recent experimental studies of resonance fluorescence of InGaAs QDs embedded in a high-quality micropillar cavity<sup>19</sup> have provided clear demonstration of excitation-induced dephasing (EID). In QD structures with no cavity coupling, the phonon-induced EID process is respon-

sible for the intensity damping of the QD excitonic Rabi rotations induced by pulsed excitation<sup>20,21</sup>. The experimental resonance fluorescence spectra in QD-cavities is similar to the characteristic Mollow triplet of a purely atomic system, but the sidebands of the triplet are found to undergo systematic spectral sideband broadening with increasing continuous-wave (cw) drives<sup>19</sup>. This drive-dependent broadening results from the interaction of the driven QD with the underlying phonon reservoir<sup>22-27</sup>. Moreover, phonon scattering processes also introduce an additional coupling mechanism between a non-resonant cavity and the QD<sup>28,29</sup>. This additional coupling depends on the QD-cavity detuning and the intrinsic parameters of the phonon bath. Cavity-QD coupling can also be used to measure the fluorescence spectra of the QD via the cavity mode which is convenient because of spectral (and possible geometrical) separation between the QD and the cavity mode. Phonon processes also play an important role in *incoherently* pumped cavity-QED systems which are known to result in off-resonant “feeding”<sup>30-37</sup> of the cavity mode, an effect which is also exists in coherently driven systems. There have been several attempts at an improved theoretical description of a semiconductor cavity-QED system to include the effects of electron-phonon scattering<sup>34,38-43</sup>. As an example, the vacuum Rabi doublet of a cavity-QED system in

the strong coupling regime also undergoes modification due to phonon coupling<sup>44</sup>; e.g., the spectral doublets—for on-resonance coupling—are *asymmetric*, especially at low temperatures which can be explained in terms of phonon-assisted processes<sup>34,41,42,45</sup>.

The complexities of a coherently-driven semiconductor cavity-QED system are best treated in a quantum master equation (ME) formalism which can be used to investigate both qualitative and quantitative changes in the Mollow spectra due to phonon-induced scattering processes. In this paper, we present two alternative ME forms which govern the evolution of the reduced density matrix, wherein we include the system-bath incoherent interaction to second order<sup>25,28,46</sup> in the system-reservoir coupling. These two MEs are termed the Nakajima-Zwanzig (NZ) form and the time-convolutionless (TC) form. To second-order in the polaron transformed system-phonon-reservoir coupling, these ME forms are equivalent to the standard Born and Born-Markov MEs, but we keep the former notation to avoid confusion with a second-Markov approximation which can be applied on the memory relaxation of the phonon reservoir. The polaron frame, obtained following a unitary polaron-transformation, allows us to study the effects of phonon dephasing on the coherent part of the Hamiltonian exactly to all orders, i.e., beyond the Born approximation. Moreover, these polaron MEs allow us to study the non-perturbative dynamics of a cavity-QED system interacting with a radiation reservoir and driven by an external cw laser field which is also under the influence of the phonon environment. The use of the polaron frame eliminates the QD-phonon coupling in the system Hamiltonian and introduces a modified QD-cavity coupling and modified radiative decay rate<sup>45,47,48</sup>. The polaron transformation also results in a spectral reduction of the QD resonance frequency. In addition, the Rabi frequency of the cw laser is renormalized by a temperature-dependent factor which accounts for the dephasing of the drive due to coupling to phonons.

The rest of our paper is organized as follows. In Sec. II we present our model Hamiltonian and derive a second-order TC (or Born-Markov) form of the ME and provide a detailed comparison with the second-order NZ (or Born) form. The computational effort necessary to solve the NZ ME is significantly more complex than the TC ME. However, for cw drives, we show that both ME forms produce identical dynamics and spectra. We also study the Markov limit of the TC ME by neglecting the memory dynamics of the phonon reservoir, and show that, for our parameters and drives, the full non-Markov solution is identical (or at least indistinguishable) to the dynamics obtained in the Markov limit. Thus we subsequently use the Markov form of the TC ME form for our remaining calculations. In Sec. III we present and discuss our numerical results of the the resonance fluorescence spectra of a coherently driven cavity-QED system with an exciton pump field; the QD linear absorption spectrum is also shown for several different bath tem-

peratures. We study the role of the temperature of the underlying phonon reservoir on the fluorescence spectra. We then explore the effects of QD-cavity detuning and identify regions where the QD-cavity coupling is particularly strong. Next, we provide an analysis of the effects of cw-laser drive and QD-cavity coupling on the spectrum and also present detailed simulations of the fluorescence spectra for various QD-cw laser detuning. We subsequently investigate EID effects by numerically extracting the spectral line widths of the phonon sidebands for various cw-laser drives. Finally, we study the dependence of QD-laser detuning on the Mollow-triplet sideband broadening (line widths). In Sec. IV, we summarise our results and present our conclusions.

## II. THEORY

### A. Model Hamiltonian

We start by introducing a model Hamiltonian which describes the QD-driven cavity-QED system where the QD interacts with a phonon reservoir and the dot is driven by a cw-laser field. Considering a single exciton (electron-hole pair), and transforming to a frame rotating with respect to the laser pump frequency,  $\omega_L$ , the model Hamiltonian is

$$H = \hbar\Delta_{xL}\hat{\sigma}^+\hat{\sigma}^- + \hbar\Delta_{cL}\hat{a}^\dagger\hat{a} + \hbar g(\hat{\sigma}^+\hat{a} + \hat{a}^\dagger\hat{\sigma}^-) + \hbar\eta_x(\hat{\sigma}^- + \hat{\sigma}^+) + \hat{\sigma}^+\hat{\sigma}^- \sum_q \hbar\lambda_q(\hat{b}_q + \hat{b}_q^\dagger) + \sum_q \hbar\omega_q\hat{b}_q^\dagger\hat{b}_q, \quad (1)$$

where  $\Delta_{\alpha L} \equiv \omega_\alpha - \omega_L$  ( $\alpha = x, c$ ) are the detunings of the exciton ( $\omega_x$ ) and cavity ( $\omega_c$ ) from the coherent pump laser frequency,  $\hat{b}_q(\hat{b}_q^\dagger)$  are the annihilation (creation) operators of the phonon reservoir,  $\hat{a}$  is the cavity mode annihilation operator,  $\hat{\sigma}^+, \hat{\sigma}^-$  are the Pauli operators of the exciton, and  $g$  is the exciton-cavity coupling strength. The pumping term,  $\eta_x$ , describes the coherent exciton excitation from the resonant cw laser field. We have included the role of phonons at the level of the independent boson model (IBM)<sup>47</sup> which is known to yield good agreement with experiments on single QDs<sup>2</sup>. A more complete description of the phonon reservoir, e.g., to allow broadening of the zero phonon line (ZPL), would require the generalization of the above system Hamiltonian to include additional processes, such as spectral diffusion, anharmonicity effects<sup>49,50</sup>, phonon scattering from interfaces<sup>51,52</sup>, and a modified phonon spectrum<sup>53</sup>. Phenomenologically, we include radiative and pure dephasing mechanisms to broaden the ZPL, and these parameters are usually known from experiments.

We seek to solve the Hamiltonian dynamics in the polaron frame<sup>2</sup>, where  $H' \rightarrow e^{-S} H e^S$ , with  $S =$

$\sigma^+ \sigma^- \sum_q \frac{\lambda_q}{\omega_q} (\hat{b}_q^\dagger - b) \cdot$ . The transformed Hamiltonian is

$$H'_{\text{sys}} = \hbar(\Delta_{xL} - \Delta_P) \hat{\sigma}^+ \hat{\sigma}^- + \hbar\Delta_{cL} \hat{a}^\dagger \hat{a} + \langle B \rangle \hat{X}_g, \quad (2a)$$

$$H'_{\text{bath}} = \sum_q \hbar\omega_q \hat{b}_q^\dagger \hat{b}_q, \quad (2b)$$

$$H'_{\text{int}} = \hat{X}_g \hat{\zeta}_g + \hat{X}_u \hat{\zeta}_u, \quad (2c)$$

with

$$\hat{B}_\pm = \exp \left( \pm \sum_q \frac{\lambda_q}{\omega_q} (\hat{b}_q - \hat{b}_q^\dagger) \right), \quad (3a)$$

$$\hat{\zeta}_g = \frac{1}{2}(\hat{B}_+ + \hat{B}_- - 2\langle B \rangle), \quad (3b)$$

$$\hat{\zeta}_u = \frac{1}{2i}(\hat{B}_+ - \hat{B}_-). \quad (3c)$$

The operators  $\hat{B}_\pm$  are coherent displacement operators of the phonon modes. Also,  $\hat{X}_g$  and  $\hat{X}_u$  are given by

$$\hat{X}_g = \hbar g (\hat{a}^\dagger \hat{\sigma}^- + \hat{\sigma}^+ \hat{a}) + \hbar \eta_x (\hat{\sigma}^- + \hat{\sigma}^+), \quad (4a)$$

$$\hat{X}_u = i\hbar g (\hat{\sigma}^+ \hat{a} - \hat{a}^\dagger \hat{\sigma}^-) + i\hbar \eta_x (\hat{\sigma}^+ - \hat{\sigma}^-). \quad (4b)$$

The thermally averaged phonon operators can be shown to obey the following:<sup>47</sup>  $\langle B \rangle = \langle B_+ \rangle = \langle B_- \rangle$ , which are explicitly defined later [see Eq. (9)]. The polaron shift, given by  $\Delta_P = \sum_q \frac{\lambda_q^2}{\omega_q}$ , accounts for the renormalization of the QD exciton resonant frequency due to coupling to the phonon modes. Henceforth we assume that the polaron shift is implicitly included in  $\omega_x$ . Note the slightly different definition of the system Hamiltonian in Eq. (2a)

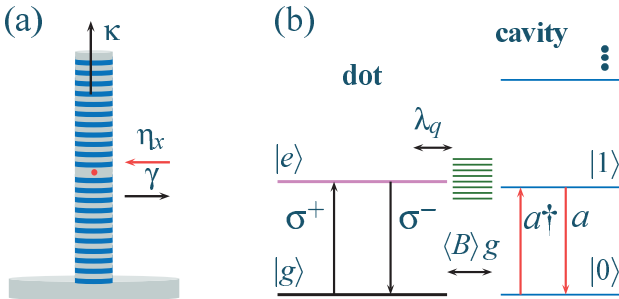


FIG. 1: (Color online) (a) Schematic of a semiconductor cavity used in cavity-QED (micropillar system), containing a coupled QD and driven by a cw laser ( $\eta_x$  from the side). The fluorescence spectra of this QD-driven system is measured via cavity emission. The emitted photons are collected from the top. Geometric and spectral decoupling of the cavity and the QD allows for much better collection of fluorescence spectra. (b) Schematic of a QD-driven cavity-QED system, where  $|e\rangle$  denotes the excited QD state,  $|g\rangle$  denotes the ground QD state. Also shown is the phonon reservoir as green (multiple) lines which is only coupled to the excited state of the QD modelled theoretically using the IBM (see text).

which is central to obtaining results in the nonperturbative regime. A detailed discussion of the reasons for the above choice of the system Hamiltonian can be found in Refs. 54,55. Figure 1 shows a schematic of the QD-cavity system [Fig. 1(a)] as well as an energy level diagram [Fig. 1(b)] showing the exciton levels, some of the phonon levels, and the cavity photon states. The exciton-cavity coupling term,  $\langle B \rangle g$ , corresponds to a coherent reduction of the bare  $g$  due to phonon interactions.

## B. Master equation

The standard approach to describe system-reservoir interactions is to derive a suitable ME in a form suitable for numerical (or analytical, if possible) solution that can include photon interactions to any arbitrary order. These MEs are usually derived using projection operator techniques such as the NZ form or the TC form<sup>46</sup>. The former approach leads to an integro-differential equation convoluted with the memory kernel which encapsulates the effects of the reservoir. However, the latter form results in a ME which is *local* in time with time-dependent superoperators acting on the reduced density matrix<sup>56–58</sup>. As mentioned before, to second order, these are the same as the standard Born and Born-Markov MEs in quantum optics.

The derivation of the ME for the reduced density matrix of the system in the NZ form starts with an equation that is written to second-order in the system-reservoir couplings (within a Born approximation)<sup>59</sup> in the interaction picture; defined with respect to  $H'_{\text{sys}} + H'_B$  as  $\tilde{H}_I(t) = e^{i(H'_{\text{sys}} + H'_{\text{bath}})t} H_I e^{-i(H'_{\text{sys}} + H'_{\text{bath}})t}$ . One obtains the following equation of motion for the reduced density operator:

$$\left. \frac{\partial \tilde{\rho}(t)}{\partial t} \right|_{\text{NZ}} = -\frac{1}{\hbar^2} \int_0^t dt' \text{tr}_B \left\{ \left[ \tilde{H}_I(t), \left[ \tilde{H}_I(t'), \tilde{\rho}(t') \rho_B \right] \right] \right\}, \quad (5)$$

where the tildes denote the operators in the interaction picture. A Markovian form of the general NZ ME, Eq. (5), to second order in the interaction terms can be derived by approximating  $\tilde{\rho}(t')$  with  $\tilde{\rho}(t)$  to obtain:

$$\left. \frac{\partial \tilde{\rho}(t)}{\partial t} \right|_{\text{TC}} = -\frac{1}{\hbar^2} \int_0^t dt' \text{tr}_B \left\{ \left[ \tilde{H}_I(t), \left[ \tilde{H}_I(t'), \tilde{\rho}(t) \rho_B \right] \right] \right\}. \quad (6)$$

This TC form eliminates the dependence of the integral on the right-hand side (RHS) on the density matrix at all previous times<sup>46,54</sup>. However, some memory (time history) effects can still exist depending upon the form of the bath interaction. A further simplification of the above form of the ME Eq. (6) is obtained by extending the upper limit of the integral to  $\infty$ . This is a *second Markov approximation* that yields a ME in the

TC Markov form, which can be further manipulated—under certain approximations—to produce an approximate phonon ME of the standard Lindblad form<sup>55</sup>.

In the interaction picture, defined with respect to the Hamiltonian  $H'_{sys} + H'_{bath}$ , we rewrite Eq. (6) as

$$\begin{aligned} \left. \frac{\partial \tilde{\rho}(t)}{\partial t} \right|_{TC} = & -\frac{1}{\hbar^2} \sum_{m=g,u} \left[ \int_0^t dt' \text{tr}_B \{ \zeta_m(t) \zeta_m(t') \rho_B \} \tilde{X}_m(t) \tilde{X}_m(t') \tilde{\rho}(t) \right. \\ & - \int_0^t dt' \text{tr}_B \{ \zeta_m(t) \rho_B \zeta_m(t') \} \tilde{X}_m(t) \tilde{\rho}(t) \tilde{X}_m(t') \\ & - \int_0^t dt' \text{tr}_B \{ \zeta_m(t') \rho_B \zeta_m(t) \} \tilde{X}_m(t') \tilde{\rho}(t) \tilde{X}_m(t) \\ & \left. + \int_0^t dt' \text{tr}_B \{ \rho_B \zeta_m(t') \zeta_m(t) \} \tilde{\rho}(t) \tilde{X}_m(t') \tilde{X}_m(t) \right], \end{aligned} \quad (7)$$

where  $\zeta_m(t) = e^{iH'_{bath}t} \zeta_m e^{-iH'_{bath}t}$ . The separation of the trace over the phonon variables is possible because we assume an initially separable density matrix consisting of the system (reduced) density matrix and the phonon bath density matrix  $\rho_B$ . We have also assumed that the full density matrix [i.e.,  $\rho_B \rho(t)$ ] remains separable at all later times. We denote  $\text{tr}_B \{ \rho_B \zeta_m(t) \zeta_m(t') \} = G_m(t-t')$  and  $\text{tr}_B \{ \rho_B \zeta_m(t') \zeta_m(t) \} = G_m(t'-t)$ , where  $G_m(t)$  are the polaron Green functions<sup>45,47</sup>:

$$\begin{aligned} G_g(t) &= \langle \hat{B} \rangle^2 (\cosh[\phi(t)] - 1), \\ G_u(t) &= \langle \hat{B} \rangle^2 \sinh[\phi(t)], \end{aligned} \quad (8)$$

and the phonon correlation function  $\phi(t)$  is defined as

$$\phi(t) = \int_0^\infty d\omega \frac{J(\omega)}{\omega^2} [\coth(\beta\hbar\omega/2) \cos(\omega t) - i \sin(\omega t)]. \quad (9)$$

We choose a phonon dispersion relation of the form  $\omega(q) \propto q e^{-q^2/2\omega_b^2}$  where  $\omega_b$  is the phonon cutoff frequency<sup>2,48</sup>. The relevant phonon spectral function  $J(\omega)$  is given by  $J(\omega) = \alpha_p \omega^3 \exp(-\omega^2/2\omega_b^2)$  where  $\alpha_p$  is the exciton-phonon coupling strength and  $\omega_b$  is the phonon cutoff frequency. We use the following parameters for our calculations: deformation potentials  $D_e - D_h = 6.5$  eV, mass density  $\rho = 5.667$  g cm<sup>-3</sup>, longitudinal sound velocity  $c_l = 3800$  m s<sup>-1</sup>. We find  $\omega_b = 1$  meV and  $\alpha_p/(2\pi)^2 = 0.06$  ps<sup>2</sup> as typical numbers for InAs/GaAs QDs<sup>38</sup>. The thermally averaged coherent phonon displacement operator  $\langle B \rangle$  and the polaron-shift  $\Delta$  can be defined in terms of the spectral function,  $J(\omega)$ , through:

$$\langle B \rangle = \exp \left[ -\frac{1}{2} \int_0^\infty d\omega \frac{J(\omega)}{\omega^2} \coth(\beta\hbar\omega/2) \right], \quad (10)$$

$$\Delta = \int_0^\infty d\omega \frac{J(\omega)}{\omega}. \quad (11)$$

Transforming back to the Schrodinger picture and changing variables from  $t - t' = \tau$ , we note that  $G_m(-\tau) =$

$G_m^*(\tau)$ , and simplify Eq. (7) as

$$\begin{aligned} \frac{\partial \rho(t)}{\partial t} = & \frac{1}{i\hbar} [H'_{sys}, \rho(t)] \\ & - \frac{1}{\hbar^2} \int_0^t d\tau \sum_{m=g,u} G_m(\tau) \hat{X}_m e^{-iH'_{sys}\tau} \hat{X}_m e^{iH'_{sys}\tau} \rho(t) \\ & + \frac{1}{\hbar^2} \int_0^t d\tau \sum_{m=g,u} G_m^*(\tau) \hat{X}_m \rho(t) e^{-iH'_{sys}\tau} \hat{X}_m e^{iH'_{sys}\tau} \\ & + \frac{1}{\hbar^2} \int_0^t d\tau \sum_{m=g,u} G_m(\tau) e^{-iH'_{sys}\tau} \hat{X}_m e^{iH'_{sys}\tau} \rho(t) \hat{X}_m \\ & - \frac{1}{\hbar^2} \int_0^t d\tau \sum_{m=g,u} G_m^*(\tau) \rho(t) e^{-iH'_{sys}\tau} \hat{X}_m e^{iH'_{sys}\tau} \hat{X}_m. \end{aligned} \quad (12)$$

The form of the TC ME derived above is local in time and can be rewritten in a compact form:

$$\begin{aligned} \frac{\partial \rho(t)}{\partial t} = & \frac{1}{i\hbar} [H'_{sys}, \rho(t)] + L(\rho) - \frac{1}{\hbar^2} \int_0^t d\tau \sum_{m=g,u} \\ & \left( G_m(\tau) [\hat{X}_m, e^{-iH'_{sys}\tau/\hbar} \hat{X}_m e^{iH'_{sys}\tau/\hbar} \rho(t)] + \text{H.c.} \right), \end{aligned} \quad (13)$$

where we have added the  $L(\rho)$  superoperators on the RHS to take into account additional dissipation processes that are necessary to obtain a complete description of the system-bath dynamics<sup>60</sup>. Defining  $\hat{\sigma}_{11} = \hat{\sigma}^+ \hat{\sigma}^-$ , then

$$\begin{aligned} L(\rho) = & \frac{\tilde{\gamma}_x}{2} (2\hat{\sigma}^- \rho \hat{\sigma}^+ - \hat{\sigma}^+ \hat{\sigma}^- \rho - \rho \hat{\sigma}^+ \hat{\sigma}^-) \\ & + \kappa (2\hat{a} \rho \hat{a}^\dagger - \hat{a}^\dagger \hat{a} \rho - \rho \hat{a}^\dagger \hat{a}) \\ & + \frac{\gamma'}{2} (2\hat{\sigma}_{11} \rho \hat{\sigma}_{11} - \hat{\sigma}_{11} \hat{\sigma}_{11} \rho - \rho \hat{\sigma}_{11} \hat{\sigma}_{11}), \end{aligned} \quad (14)$$

where  $2\kappa$  is the cavity decay rate,  $\gamma'$  is the pure dephasing rate, and  $\tilde{\gamma}_x = \gamma_x \langle B \rangle^2$  is the radiative decay rate<sup>55,64</sup>. Note that we include additional pure dephasing effects beyond the IBM, e.g., perhaps caused by quadratic QD-acoustic phonon and phonon-phonon interactions<sup>61,62</sup>, with a rate  $\gamma'$ ; this pure dephasing contribution to the ZPL broadening is known to increase linearly with increasing temperatures<sup>22,63</sup>.

The timescales associated with the phonon and radiative processes are substantially different<sup>64</sup>. Phonon processes happen at picosecond timescales whereas radiative timescales are smaller by (typically) at least an order of magnitude<sup>41</sup>. This results in a substantial simplification of the ME derived above in the TC form. Extending the upper limit of the integral ( $t \rightarrow \infty$ ), Eq. (13) can be rewritten as

$$\begin{aligned} \frac{\partial \rho(t)}{\partial t} = & \frac{1}{i\hbar} [H'_{sys}, \rho(t)] + L(\rho) - \frac{1}{\hbar^2} \int_0^\infty d\tau \sum_{m=g,u} \times \\ & \left( G_m(\tau) [\hat{X}_m, e^{-iH'_{sys}\tau/\hbar} \hat{X}_m e^{iH'_{sys}\tau/\hbar} \rho(t)] + \text{H.c.} \right). \end{aligned} \quad (15)$$



We refer to this as in TC Markov form. The validity of extending the time limits of the integration to  $\infty$  depends on the ensuing system dynamics introduced by the external drive, and the cavity coupling (through  $g$ ), with respect to the phonon bath relaxation time. For instance, a cavity-QED system driven by a fast pulse may require a fully non-Markovian treatment to obtain a correct description of nonradiative processes. Non-Markovian effects within the polaron frame ME are likely to affect the population dynamics only at extremely short times and the difference between non-Markov and Markov dynamics vanish at longer timescales<sup>25</sup>. For the present system of interest (with cw drives), the Markov approximation is found to be an excellent approximation as will be shown numerically in the next section.

Using similar steps as above, Eq. (5) leads to a ME of the NZ form that involves integrating the system dynamics over all previous times, given by<sup>45,54</sup>

$$\frac{\partial \rho(t)}{\partial t} = \frac{1}{i\hbar} [H'_{\text{sys}}, \rho(t)] + L(\rho) - \frac{1}{\hbar^2} \int_0^t d\tau \sum_{m=g,u} (16) \\ (G_m(\tau) [\hat{X}_m, e^{-iH'_{\text{sys}}\tau/\hbar} \hat{X}_m \rho(t-\tau) e^{iH'_{\text{sys}}\tau/\hbar}] + \text{H.c.}).$$

The above ME is non-local in time and generates equations of motion which are convoluted in time.

We note that the validity of the Born approximation in Eq. (15) depends on the physical parameters of the cavity-QED system. A general condition for the validity of the second-order Born approximation has been derived by McCutcheon and Nazir and is given by  $\frac{\eta_x^2}{\omega_b^2} (1 - \langle B \rangle^4) \ll 1$ . A similar condition for the validity of the Born approximation for the cavity-QED system is as follows:  $\frac{\eta_x^2}{\omega_b^2} (1 - \langle B \rangle^4) \ll 1$ ,  $\frac{g^2}{\omega_b^2} (1 - \langle B \rangle^4) \ll 1$  and  $\frac{\eta_x g}{\omega_b^2} (1 - \langle B \rangle^4) \ll 1$ , which are well satisfied for the parameter regimes used in our studies below. This suggests that the a second-order Born approximation is perfectly valid for our present system (remembering that nonperturbative coupling effects beyond second-order Born are captured within the polaron transform itself).

Also note that a ME describing the cavity-QED dynamics can also be derived without using the polaron transformation<sup>65</sup>. This is effectively a *weak-coupling* theory which only includes exciton-phonon interactions to second-order and is known to breakdown for higher temperatures and strong exciton-phonon couplings<sup>25</sup>. With cavity coupling, these weak phonon-coupling failures can become even stronger<sup>28,55</sup>. A more general approach using a variationally-optimized master equation has also been recently developed in Ref. 66. The variational master equation includes nonperturbative phonon effects and multi-phonon processes over a wide range of parameters (especially important for very large driving fields). However, for purposes of this paper, the polaron transformation suffices as the coherent laser drives are much smaller than the phonon cutoff frequency.

With coherent excitation, we define the incoherent fluorescence spectra associated with cavity mode emission

( $S_c$ ), and the QD emission ( $S_x$ )<sup>64</sup>, as follows:

$$S_c(\omega) \propto \frac{\kappa}{\pi} \lim_{t \rightarrow \infty} \text{Re} \left[ \int_0^\infty d\tau (\langle \hat{a}^\dagger(t+\tau) \hat{a}(t) \rangle - \langle \hat{a}(t) \rangle \langle \hat{a}^\dagger(t) \rangle) e^{i(\omega_L - \omega)\tau} \right], \quad (17)$$

$$S_x(\omega) \propto \frac{\tilde{\gamma}_x}{\pi} \lim_{t \rightarrow \infty} \text{Re} \left[ \int_0^\infty d\tau (\langle \hat{\sigma}^+(t+\tau) \hat{\sigma}^-(t) \rangle - \langle \hat{\sigma}^+(t) \rangle \langle \hat{\sigma}^-(t) \rangle) e^{i(\omega_L - \omega)\tau} \right]. \quad (18)$$

Note the phase term  $e^{\phi^*(t)}$  in the definition of the QD spectra,  $S_x(\omega)$ , which arises due to the polaron transformation and accounts for the dephasing of the exciton coherence in the phonon reservoir. In the polaron frame, the QD autocorrelation function  $\langle \hat{\sigma}^+(t+\tau) \hat{\sigma}^-(t) \rangle$  is transformed to  $\langle \hat{\sigma}^+(t+\tau) \hat{B}_+(t+\tau) \hat{\sigma}^-(t) \hat{B}_-(t) \rangle$ . The trace over the phonon degrees of freedom and the QD Hilbert space can then be easily evaluated as the Hilbert space is separable in the polaron frame. It is also useful to define the QD susceptibility (or polarizability),  $\chi(\omega)$ , that describes the linear response of the QD in the presence of phonon coupling and phenomenological dissipation only (i.e., not coupled to the cavity mode,  $g \simeq 0$ , and driven by a linear optical field). This polarizability function is obtained from

$$\chi(\omega) \propto \int_0^\infty d\tau \langle \hat{\sigma}^-(\tau) \hat{\sigma}^+(0) \rangle e^{\phi(\tau)} e^{i(\omega_x - \omega)\tau}. \quad (19)$$

The simple form of  $\chi(\omega)$  obtained above, with the phonon contribution described by the phonon correlation function  $\phi(t)$ , is due to the polaron transformation. To obtain the bare QD response function (polarizability), the expectation is evaluated in the absence of any QD-cavity coupling, and we excite the QD exciton with a linear (weak), incoherent pump process, via the Lindblad superoperator:  $\frac{P_x}{2} (2\hat{\sigma}^- \rho \hat{\sigma}^+ - \hat{\sigma}^+ \hat{\sigma}^- \rho - \rho \hat{\sigma}^+ \hat{\sigma}^-)$ . The system Hamiltonian  $H'_{\text{sys}}$  defined above describes the QD-phonon interaction in the polaron frame. The linear absorption spectra  $\chi''(\omega)$  is defined as the imaginary part of the QD susceptibility  $\chi(\omega)$ . It is interesting to recognize that the phonon correlation function  $\phi(t)$  is explicitly present in the definition of the  $S_x$  and  $\chi(\omega)$ . The dynamics of equations we solve is effectively Markovian in the polaron frame, which is much easier to work with from a numerical viewpoint. However, the transformation back to the original frame reintroduces the non-Markov phonon dynamics through the phonon correlation function  $\phi(t)$ . Note also that the cavity spectral function does not depend directly on  $\phi(t)$ , so the cavity spectrum may not depend at all on any non-Markovian dynamics (at least from a mathematic viewpoint).

The spectra are calculated by the numerical solution of the Markovian ME driven by a steady-state pump  $\eta_x$ . The ME is solved in a Jaynes-Cummings basis with states  $|0\rangle$ ,  $|1L\rangle$ ,  $|1U\rangle$ ,  $|2L\rangle$ ,  $|2U\rangle$  and so on. Denoting the photon states  $|n\rangle$ , with  $n = 0, 1, 2, \dots$ , and exciton states  $|e/g\rangle$ , the Jaynes-Cummings basis states

are given by  $|0\rangle = |g\rangle|0\rangle$ ,  $|1L\rangle = 1/\sqrt{2}(|g\rangle|1\rangle - |e\rangle|0\rangle)$ ,  $|1U\rangle = 1/\sqrt{2}(|g\rangle|1\rangle + |e\rangle|0\rangle)$ , etc. The system is initialized with the exciton and cavity in the ground state which then evolve, in the presence of a cw pump, to a dynamical steady state. Using the quantum regression formula<sup>59</sup>, we subsequently compute the relevant two-time correlation function whose decay is initialized by the steady state population and coherences. The calculations are performed partially using the *quantum optics toolbox* by Tan<sup>67</sup>. We note that, in general, it is vital to include multiphoton effects to get the correct (numerically converged in the photon number) fluorescence spectra; though a one photon basis is (obviously) enough to obtain the linear absorption. We have verified the need for multiphoton effects elsewhere and find that the truncation of the hierarchy of the photon states to two-photon-correlations (two photon states) is sufficient for exciton driving<sup>28</sup>. A broader discussion of the role of multiphoton processes, especially in the context of power broadening, is presented in Ref. 55.

### III. RESULTS AND DISCUSSION

In this section, we present and discuss our numerical results.

#### A. Linear absorption spectra

In Fig. 2 we show the linear absorption spectra of the QD,  $\chi''(\omega)$ , for two different temperatures of the phonon bath. The absorption spectra in the vicinity of

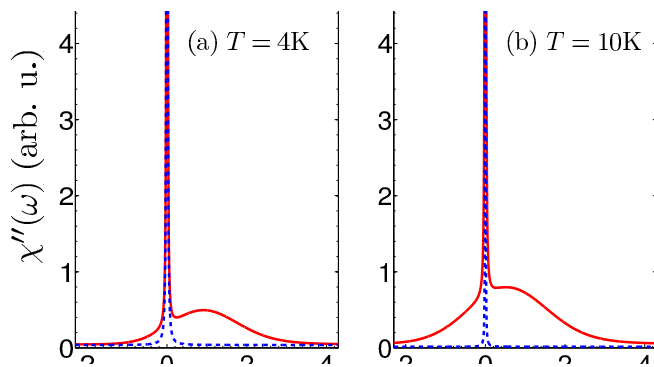


FIG. 2: Linear absorption spectra of the QD,  $\chi''(\omega)$ , for two different phonon bath temperatures: (a)  $T = 4$  K and (b)  $T = 20$  K; red-solid line includes phonon coupling and blue-dashed line has no phonon coupling; QD decay parameters  $\tilde{\gamma}_x = 1$   $\mu\text{eV}$  and  $\gamma' = 2$   $\mu\text{eV}$  are used in both plots. The asymmetry in the absorption spectra due to the phonon reservoir is clearly seen, especially at lower temperatures. The absorption spectra becomes more symmetric about the ZPL with increasing temperatures. Also note the broadening of the ZPL due to radiative decay and pure dephasing of the QD exciton.

the QD resonance is dominated by the IBM spectral function which allows the dot to absorb photons by phonon-assisted processes. In the absence of any phonon coupling (blue dashed lines in Fig. 2), the absorption spectrum is a simple Lorentzian whose width is terminated by radiative broadening and pure dephasing (the ZPL). The asymmetry in the absorption spectra in the presence of phonons is clearly seen at low temperatures, which is caused by different probabilities to absorb or emit a phonon; the latter process is more likely at low temperature. This asymmetry naturally decreases with increasing temperatures, and the ZPL typically further broadens.

#### B. TC vs NZ master equation solutions

In Fig. 3 we compare the population dynamics generated by NZ ME, TC ME and the TC Markov ME. We find that all three ME forms produce identical results for the evolution of the cavity and QD populations, defined as  $n_c(t) = \langle \hat{a}^\dagger \hat{a}(t) \rangle$  and  $n_x(t) = \langle \hat{\sigma}^+ \hat{\sigma}^-(t) \rangle$ . We also compare the fluorescence spectra as shown in Fig. 4 (defined in the previous section), generated by the respective

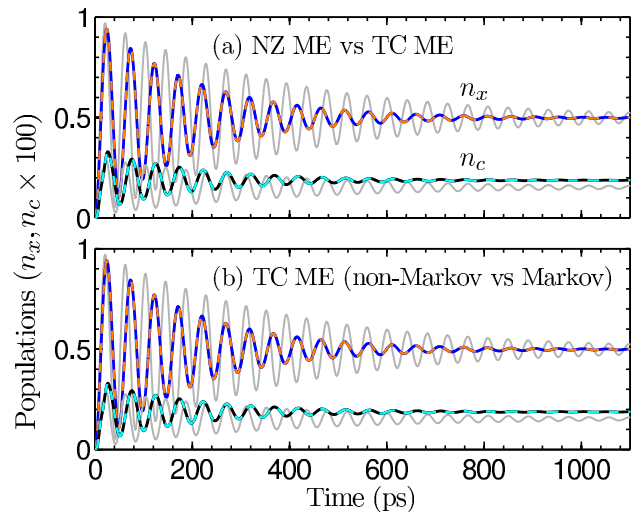


FIG. 3: (a) Comparison of the population dynamics generated by the NZ and the TC form of the ME, both to second-order in the system-phonon-reservoir coupling. The upper blue (dark) solid-line is the QD exciton population  $n_x$  using the NZ solution, and the orange (light) dashed-line is the TC ME solution. We also plot the cavity mode population  $n_c(t)$ . The grey (light) solids are the exciton and the cavity mode populations in the absence of any phonon coupling. In (b) we compare the TC and the TC Markov dynamics generated by the MEs. The blue-solid line shows the exciton population  $n_x(t)$  with the TC ME evolution, while the orange-dashed line is the dynamics generated by the TC Markov ME form. All the plots were obtained by truncating the hierarchy of equations of motion at the one-photon limit, and using a phonon bath temperature of  $T = 10$  K. The cavity-QED system parameters were  $\tilde{\gamma}_x = 1$   $\mu\text{eV}$ ,  $\kappa = 50$   $\mu\text{eV}$ ,  $\gamma' = 2$   $\mu\text{eV}$ ,  $g = 20$   $\mu\text{eV}$  and  $\langle B \rangle (T = 10 \text{ K}) = 0.85$ .

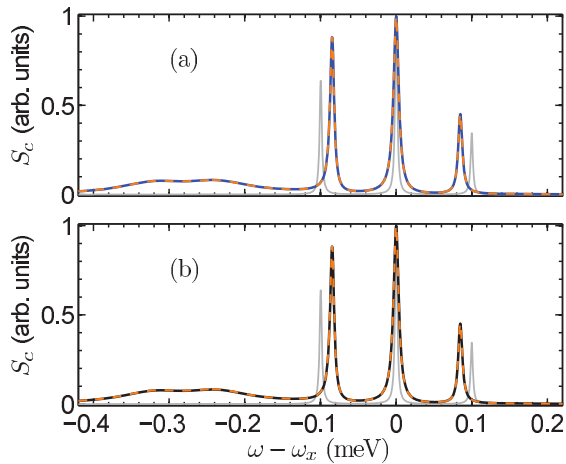


FIG. 4: (a) Corresponding cavity-emitted resonance fluorescence spectra from Fig. 3. The blue-solid line is the cavity-emitted fluorescence spectra computed using the NZ form and the orange-dashed line is the spectra generated by the TC ME. The grey solid shows the spectrum in the absence of any phonon coupling. In (b) we compare the spectra generated by the TC and TC Markov ME results.

MEs, which are again found to be identical (or indistinguishable). Hence, in remainder of the paper we use the TC Markov form of the ME as it is much easier to work with and justified here to be an excellent approximation.

Note that for numerical convenience, these numerical results (displayed in Figs. 3-4 only) were obtained by truncating the hierarchy of equations of motion at the one photon limit because of the computational complexity of solving the NZ ME form. However, all the results discussed in the subsequent sections use the TC ME with the required (i.e., numerically converged) number of multiphoton processes; so the spectrum will be seen to qualitatively change, especially near the cavity resonance (see Ref. 28 for more details).

### C. QD-cavity detuning dependence

In Fig. 5 we study the detuning dependence of the cavity-emitted resonance fluorescence spectra for different QD-cavity detunings. The fluorescence spectra are clearly asymmetric with respect to the cavity mode detuning. This behaviour is drastically different to simple Lorentzian systems which would yield symmetric Mollow spectra. Cavity mode emission is enhanced when the QD is placed to the right of the cavity mode as the cavity-QD coupling is further strengthened by phonon emission processes. At a detuning of  $\pm 1$  meV, the red detuned cavity mode peak is found to be about double that of the blue detuned cavity mode peak, which is consistent with the experimental data (using incoherent excitation) shown by Hennessy *et al.*<sup>30</sup>. Also note that the cavity-mode peak initially increases, relative to the Mollow triplet, as the

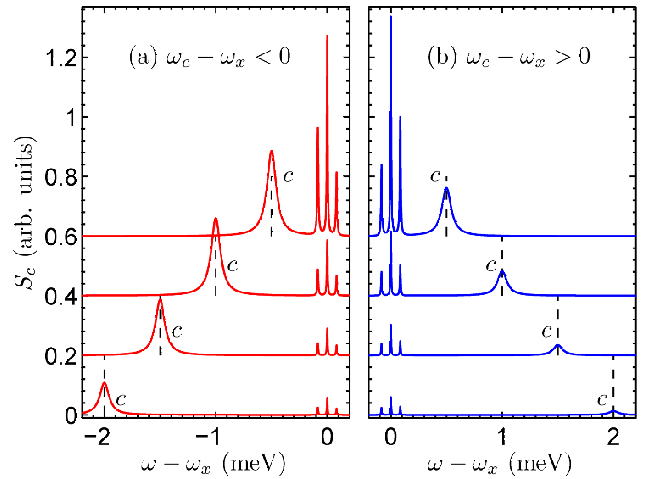


FIG. 5: Detuning dependence of the cavity-emitted resonance fluorescence spectra for different QD-cavity detunings. The other parameters are the same as in Fig. 3, again with the phonon bath temperature at  $T = 10$  K. In (a) the red lines denote the cavity-emitted fluorescence spectra when the cavity is detuned to the left of the QD. In (b) the blue lines denote the same spectra when the cavity is detuned to the right of the QD. Note that all the spectra are normalized relative to the first spectrum on the top left.

QD exciton is red detuned from the exciton; but eventually decreases for large QD-cavity detunings—essentially following the phonon spectral function. This suggests that the coupling between the QD and the cavity is optimum at a particular detuning and is determined by the QD-phonon coupling strength and the intrinsic spectral properties of the phonon reservoir. This observation is significant for experimentalists as it suggests that off-resonance cavity-QED physics is best studied at a particular QD-cavity detuning where the mode emission is maximized. Note that the emission at the cavity mode frequency is eventually suppressed at very large QD detunings  $\Delta_{cx} \simeq \pm 5$  meV, which is in agreement with recent experimental observations on site controlled QDs in cavities<sup>42</sup>. The maximum coupling between the QD and the cavity also depends on temperature, i.e., the QD-cavity detuning at which the QD-cavity mode coupling is maximum increases with temperature.

It is interesting to note that the detuning dependence of the spectra closely follows the spectral characteristics of the phonon correlation function. An intuitive way to understand this detuning dependence is using effective phonon rates in a Lindblad-type description<sup>55</sup>, which are similar to the cavity-feeding rates introduced by Hohenester<sup>40</sup>. These phonon scattering rates are related to the Fourier component of the phonon correlation function at the QD-cavity mode detuning. The same type of feature can be seen in the asymmetry of the sidebands of the vacuum-Rabi doublet in an incoherently pumped strongly coupled QD-cavity system<sup>42</sup>. Here, the asymmetry of the doublet depends closely on the spectral charac-

teristics of the phonon correlation function. Hence, these features in the fluorescence and linear spectra (with incoherent excitation) reveal subtle details of the underlying phonon reservoir, which can be probed as a function of the exciton-cavity detuning. Coherently excited systems, however, are much cleaner to study, since for incoherent excitation one never really knows the details of the pumping scenario.

#### D. Temperature dependence

In Fig. 6 we investigate the temperature dependence of the resonance fluorescence spectra and also analyse the role of one-phonon scattering versus multiphonon scattering. In Fig. 6(a), we study a red detuned cavity mode, where the grey-solid lines denote the one-phonon limit of the full polaron cavity-emitted spectra which is shown with the red-solid line. In Fig. 6(b), we study the QD exciton spectra, where the full-polaron QD spectra is now plotted as the blue-solid lines. The one-phonon limit of the full-polaron master equation is obtained by a perturbative expansion of the relevant phonon correlation functions to lowest order. Namely, we approximate  $G_g(\tau) \simeq 0$  and  $G_u(\tau) \simeq \phi(t)$ . The TC Markov ME is then solved numerically for the above choice of phonon correlation functions to study the fluorescence spectra in the one-phonon limit. We highlight that that  $\langle B \rangle \simeq 1$  in this limit which suggests that one-phonon processes do not renormalize the Rabi frequency of the cw-laser drive,  $\eta_x$ , or the QD-cavity coupling constant  $g$ . Further discussions of the temperature dependence of the cavity-emitted spectra can be found in Ref. 28.

We first observe that the emission at the cavity mode relative to the emission at the QD frequency increases with temperature. This is due to enhanced exciton-cavity coupling which increases with temperature. At high temperatures, we observe that the fluorescence spectrum is dominated by the emission at the mode frequency and the Mollow triplet at the QD resonance frequency is essentially suppressed. The Mollow triplets are increasingly broadened with temperature due to increased EID. At low drives, EID-induced broadening can dominate the well separated triplet structure and give rise to a homogeneously broadened Lorentzian centred at the QD frequency. The exciton-emitted fluorescence spectra, however, is distinctly different to the cavity-emitted spectra. Most notable is the lack of any emission at the mode frequency. Other pertinent differences are discussed in the following subsection.

The discrepancy between the one-phonon and full-polaron solution of the TC ME increases with temperature, and the one-phonon solution is found to overestimate the full-polaron solution. Since the one-phonon truncation for the full polaron theory does not renormalize the cw laser Rabi frequency, the locations of the triplets are identical to that for the case of no phonons. Hence a full polaron theory can be essential to find the

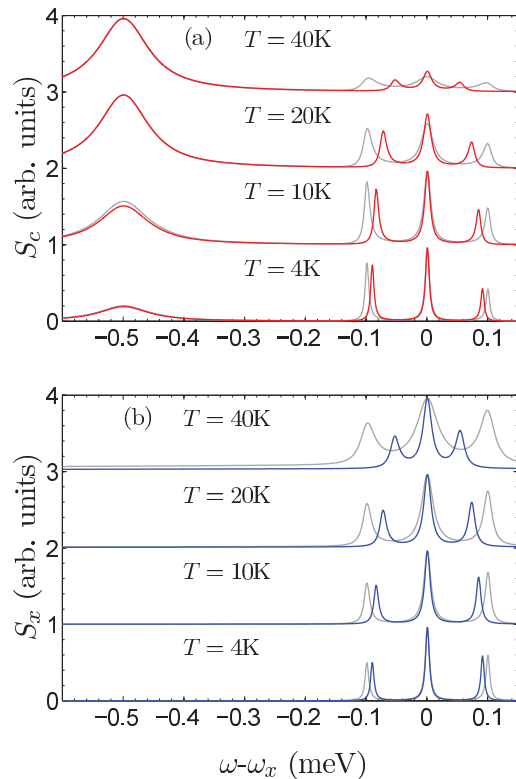


FIG. 6: Temperature dependence of the (a) cavity-emitted resonance fluorescence spectra and (b) exciton-emitted resonance fluorescence spectra for different temperatures of the phonon reservoir. Also studied is the role of one-phonon vs multiphonon (full polaron) processes on the fluorescence spectra. The QD-cavity detuning,  $\Delta_{cx} = -0.5$  meV, with the phonon reservoir at temperatures,  $T = 4$  K,  $T = 10$  K,  $T = 20$  K, and  $T = 40$  K, respectively.

correct center frequencies of the Mollow triplet resonances. Moreover, the discrepancy between the sideband locations increases with increasing temperature. These results suggest that a simple atomiclike ME would drastically fail in the present semiconductor cavity-QED excitation regime, and one must include the effects of phonon coupling.

#### E. Resonance fluorescence spectra versus pump

In Fig. 7 we study the normalized resonance fluorescence spectra for different QD-cavity detunings for various cw laser drives and dot-cavity couplings at a fixed temperature of the phonon reservoir. We observe from Fig. 7(a) and Fig. 7(c) that the relative emission at the cavity mode frequency for the cavity-emitted fluorescence spectra increases with increasing drive which can be explained by noting the enhanced coupling between the cavity mode and the QD as the low energy component is pushed closer to the cavity mode frequency. The triplet component which is proximal to the cavity mode has a



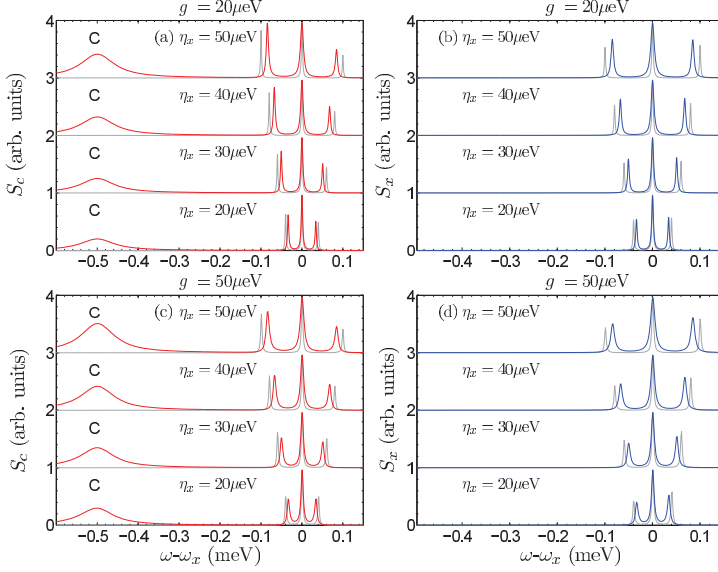


FIG. 7: Resonance fluorescence spectra for various cw-laser drives and two different exciton-cavity coupling  $g$ . The phonon reservoir at  $T = 10$  K.  $\Delta_{cx} = -0.5$  meV,  $\tilde{\gamma}_x = 1$   $\mu$ eV,  $\kappa = 50$   $\mu$ eV and  $\gamma' = 2$   $\mu$ eV. In Figs. (a) and (b) we study the cavity-emitted and exciton-emitted resonance fluorescence spectra for exciton-cavity coupling  $g = 20$   $\mu$ eV with various cw-laser driving  $\eta_x$  which are denoted as red-solid and blue-solid lines respectively. Also plotted are the grey-solid lines which are the corresponding fluorescence spectra in the absence of any phonon coupling. In Figs. (c) and (d) we study the cavity-emitted and exciton-emitted resonance fluorescence spectra for exciton-cavity coupling  $g = 50$   $\mu$ eV with similar parameters as in Figs. (a) and (b).

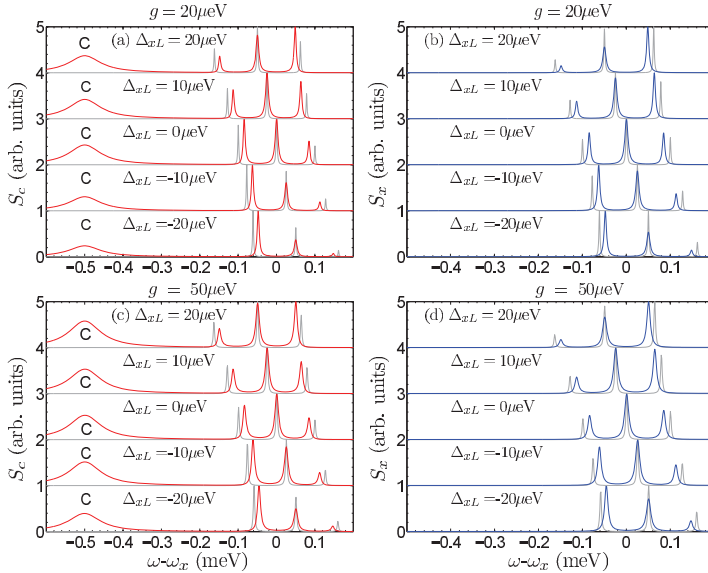


FIG. 8: Similar to Fig. 7, but with  $\eta_x$  fixed at 50  $\mu$ eV and for different exciton-cw laser detunings  $\delta_{xL}$ . In Figs. (a) and (b) we study the resonance fluorescence spectra for QD-cavity coupling  $g = 20$   $\mu$ eV with various exciton-laser detunings respectively plotted as red-solid and blue-solid lines. Also plotted are the fluorescence spectra in the absence of any phonon coupling as grey-solid lines. In Figs. (c) and (d) we study the fluorescence spectra for exciton-cavity coupling  $g = 50$   $\mu$ eV with identical detunings and cw laser drives as in Figs. (a) and (b).

higher spectral weight than the distant component which is due to stronger relative coupling with the cavity mode. However, we note that the asymmetry in the spectral weights decreases for larger  $g$  as both the proximal and the distant component of the triplet are more or less equally coupled to the cavity mode. Also note the increased broadening of the sideband with increasing  $g$ <sup>28</sup>.

Apart from the lack of any emission at the mode frequency in the QD emission spectra, the asymmetry in the Mollow triplets in the QD measured spectra is substantially smaller than the cavity emitted spectra. Furthermore, the high energy component of the triplet has a larger relative spectral weight than the low energy component. This asymmetry in the sidebands spectral weights increase with increasing  $g$  and cw-laser drive  $\eta_x$ . Interestingly, these features in the asymmetry of the sidebands are not mainly due to phonon-induced effects as they are present even in the absence of phonons. Thus

these are primarily cavity-QED effects and are easy to understand in terms of relative coupling with the cavity mode. The low-energy component of the triplet is closer to the cavity mode and couples more strongly with it. Finally, we note that the line width broadening is larger in the presence of phonons which is primarily due to stronger QD-cavity coupling mediated by phonon-assisted effects.

#### F. Fluorescence spectra with an off-resonance cw drive

In Fig. 8 we study the the cavity-emitted spectra and exciton-emitted spectra for different exciton-laser detunings and exciton-cavity couplings  $g$ , with the phonon reservoir at  $T = 10$  K. We first note that, unlike the case of resonance fluorescence (see Fig. 7), the relative spectral

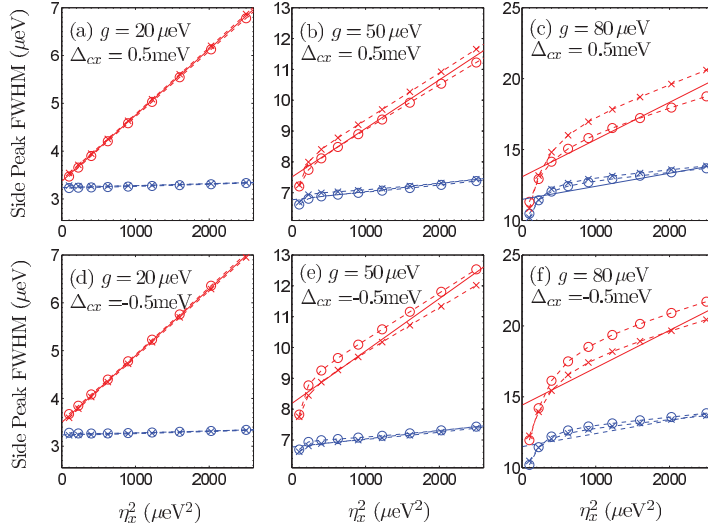


FIG. 9: Study of the numerically extracted FWHM of the on-resonance Mollow triplet for various QD-cavity detunings and QD-cavity couplings as a function of the square of the Rabi frequency  $\eta_x$ . In Figs. (a)-(c) we study the FWHM of the sidebands of the fluorescence spectrum for  $\Delta_{cx} = 0.5$  meV. The red data is with full phonon coupling and the blue data is for no phonon coupling. The crosses denote the high frequency and the circles denote the low frequency component of the Mollow triplet. Also plotted as a solid line with corresponding color is the best linear fit to the data. In Figs. (d)-(f) we study the FWHM of the sidebands of the fluorescence spectrum for  $\Delta_{cx} = -0.5$  meV and identical parameters as in the above set of plots.

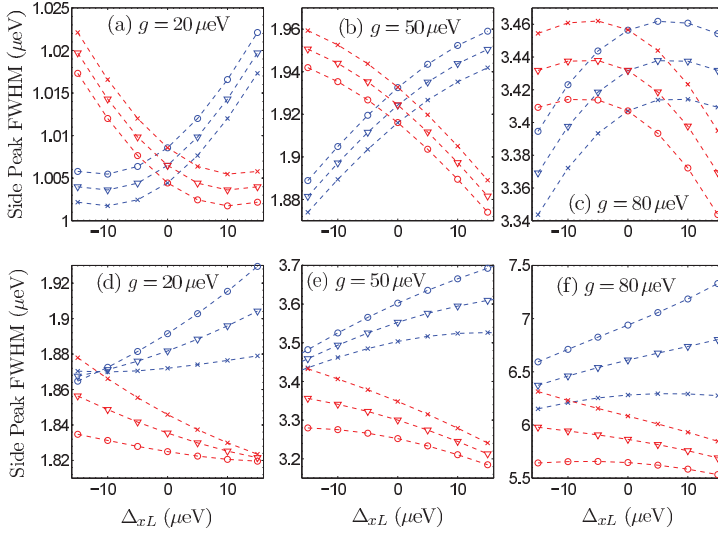


FIG. 10: Study of the numerically extracted FWHM of the off-resonance Mollow triplet for different QD-cavity detunings and couplings as a function of the QD-laser detuning  $\delta_{xL}$ . In Figs. (a)-(c) we study the FWHM of the sidebands of the fluorescence spectrum in the absence of phonons with QD-cavity couplings  $g = 20$   $\mu$ eV,  $g = 50$   $\mu$ eV and  $g = 80$   $\mu$ eV, respectively. The red data is with  $\Delta_{cx} = 0.5$  meV and the blue data is for  $\Delta_{cx} = -0.5$  meV. The crosses denote the high frequency and the circles denote the low frequency component of the Mollow triplet. The triangles are the average of the two sideband FWHM. In Figs. (d)-(f) we study the FWHM of the sidebands of the fluorescence spectrum with the phonon reservoir at  $T = 10$  K.

weights of the Mollow triplets are also determined by the exciton-cw laser drive detuning. The high-energy component of the triplet has larger relative spectral weight if the cw-laser is detuned to the right of the exciton (higher energies). Conversely, the low-energy component of the triplet has larger relative spectral weight if the cw-laser is detuned to the left of the exciton (lower energies). This observation is also valid for the exciton-emitted fluorescence spectra. An off-resonant cw-laser drive shifts the entire triplet with a corresponding shift in the location of the sidebands. A positive exciton-cw laser detuning shifts the triplet structure further away from the cavity mode but increases the spectral weight in the high energy sideband and reduces the interaction with the cavity mode. A negative exciton-cw laser detuning shifts the triplet structure towards the cavity mode and increases the spectral weight in the low energy sideband with increased interaction with the cavity mode due to reduced effective spectral detuning between the exciton and the cavity mode. Interestingly, the asymmetry in the

spectral weights is suppressed with increasing QD-cavity coupling as seen by comparing, e.g., the relative weights in Figs. 8(a)-8(c). The enhanced exciton-cavity interaction, overrides, to some extent the effects of the spectral shift induced by the off-resonant drive. Finally, note that phonon coupling enhances the asymmetry in the relative spectral weights of the Mollow triplets due to enhanced exciton coupling and reduced sideband splitting.

### G. FWHM (line width) of the Mollow sidebands

We next study the broadening of the Mollow sidebands for various excitation regimes.

In Fig. 9 we show the numerically extracted FWHM of the Mollow triplet peaks for various exciton-cavity detunings and exciton-cavity couplings as a function of the square of the Rabi frequency  $\eta_x$ . Clear signature of EID as demonstrated by the linear dependence of FWHM on the square of the Rabi frequency is seen—for low

QD-cavity couplings [Figs. 9(a) and 9(d)]. These two plots have opposite QD-cavity detunings, and EID is marginally larger when the cavity mode is detuned to the left of the QD due to increased phonon-induced coupling between the exciton and the cavity mode. This general trend of EID increasing linearly with the square of the Rabi frequency which is in agreement with recent experiments performed in semiconductor micropillars<sup>19</sup>. Increasing the QD-cavity coupling  $g$  also increases the FWHM of the sidebands due to stronger coupling between the QD and the cavity and enhanced emission into the cavity mode [Figs. 9(b) and 9(e)]. The dependence at higher QD-cavity couplings is nonlinear especially at low drives [Figs. 9(c)-9(f)]. We also find a linear increase in the FWHM as a function of the square of cw laser drive even in the absence of phonon coupling, primarily for large QD-cavity couplings [Figs. 9(c)-9(f)]. This effect can be attributed to enhanced emission into the cavity mode which is enhanced with increasing drive and broadens the triplet. Also note that there is a notable difference in the broadenings of the low-energy and high-energy components of the triplet in the presence of phonons. The triplet component proximal to the cavity mode shows larger broadening which increases with the QD-cavity coupling  $g$ .

In Fig. 10 we study the numerically extracted FWHM of the off-resonance Mollow triplet as a function of the exciton-laser detuning  $\delta_{xL}$ . We first note that coupling to phonons introduces additional broadening of the sidebands as expected due to EID effects and can be seen from the differences in magnitudes between the plots in the top panel and the bottom panel. Also note that the two sidebands of the triplet are broadened by different amounts which is governed primarily by the proximity of the sideband to the cavity mode. In the absence of any phonon coupling, the Mollow component which is closer to the cavity mode is broadened more due to enhanced emission into the cavity. Also, the difference in the broadening of the high energy and the low energy components of the triplet increases with temperature. There is a noticeable difference in the broadening of the sidebands in the presence of phonons. We find an enhancement in the FWHM broadening when the cw laser drive is spectrally located between the cavity mode and the exciton mode. In contrast, there is substantial suppression of FWHM if the cw laser is detuned in the other direction relative to the exciton-cavity detuning. This suggests that phonons enhance the broadening process in the first scenario as it allows for an additional mechanism for enhanced emission into the cavity mode.

Recent experiments in semiconductor micropillars<sup>19</sup> have noted a distinct spectral narrowing of both the high energy and the low energy sideband of the Mollow triplet with increasing exciton-cw laser detuning. This behavior is quite contrary to what is obtained (and expected) from a phonon-based EID model, as larger exciton-laser detunings increase the sideband splitting which is associated with an increase in the generalized Rabi frequency;

though a decrease in the Rabi frequency was also noticed as a function of detuning<sup>19</sup>. On the other hand, more recent experimental data obtained for weakly coupled QD-cavity systems find the opposite dependence on the exciton-laser detuning wherein the FWHM of the off-resonance Mollow triplet is found to increase with the QD-laser detuning<sup>68</sup>. Part of this anomaly can perhaps be attributed to additional detuning-dependent pure dephasing mechanisms<sup>19</sup>. Further investigations and a closer collaboration between experiments and theory are likely required to understand these trends in more detail.

#### IV. CONCLUSIONS

We have presented a detailed theoretical analysis of the cavity-emitted and exciton-emitted fluorescence spectra of a cavity-QED system under resonant and off-resonant excitation of the QD exciton. The fluorescence spectra were assumed to be collected via the cavity or exciton decay and we considered the cavity mode both on-resonance and off-resonance with the QD drive. The fundamentally distinctive feature of the semiconductor QD system we emphasize is its interaction with the acoustic phonons which we model at a microscopic level. We derived a TC ME in the polaron frame to study the fluorescence spectra, and we showed that it produces identical results to a NZ ME solution (the latter being significantly more difficult to solve numerically). This inherently nonperturbative treatment of the effects of QD exciton, acoustic phonons, cavity and the cw laser field on the coherent part of the Hamiltonian was accomplished by a suitable choice of the decomposition of the system Hamiltonian. A polaron transformation was adopted that retains coherent phonon coupling to all orders, while introducing a suitable (modified) system-bath-interaction with which to perform perturbation theory that is accurate to second order.

We subsequently investigated the spectral FWHM of the Mollow triplet sidebands for various QD-cavity detunings and QD-cavity couplings as a function of the square of the Rabi frequency, and obtained unambiguous signatures of phonon-induced EID in accordance with recent experiments. We also studied the FWHM of the off-resonance Mollow triplet as a function of the exciton-laser detuning. The interaction of the QD with the phonon reservoir was found to introduce distinctively different features in the fluorescence spectra exemplified by emission at the cavity mode and additional spectral broadening effects. With a deliberate detuning between the driving laser and the exciton, our theoretical results predict further broadening which is a prediction that is in disagreement with recent experiments in micropillars<sup>19</sup>—which suggest a spectral narrowing of sidebands with increasing exciton-laser detuning. Nevertheless, as mentioned above, recent experiments also show a spectral broadening with exciton-laser detuning<sup>68</sup>. The origin of these trends remain somewhat mysterious and clearly re-

quire closer systematic investigation between theory and experiment. The possible role of detuning-independent pure dephasing also merits further study in this context as relative magnitudes of pure dephasing and the QD radiative decay rate determine the curvature of the plot of FWHM of the off-resonant fluorescence sideband as a function of QD-laser detuning. Additional contributions from phonon damping processes and higher order QD-phonon interactions may further influence the underlying physics of this detuning-dependent EID.

The main focus of this work was to study EID and other phonon-induced scattering effects (such as exciton cavity coupling) in a QD-driven system which is observed through fluorescence either via the cavity mode or the QD. The subtle differences between the characteristics of the cavity-emitted spectra or the QD-emitted spectra help to shed light on the underlying physics of these intriguing cavity-QED system; though it is experimentally much easier to collect the fluorescence signal through an off-resonance cavity mode. The spectral separation between the QD and the cavity allows good elimination of the very strong coherent component of the resonance fluorescence (the Rayleigh scattering component). It is also instructive to perform the reverse measurement process wherein a cavity mode is driven by a cw-laser and the fluorescence signal is measured via an off-resonant QD. Detailed discussions of this system will be presented elsewhere. However, it is likely that phonon-induced EID effects would be quite different in a cavity-driven system since the cavity mode is not directly coupled to the phonon reservoir<sup>55</sup>. Preliminary research suggests that EID in a cavity-mode driven system is unlikely to have a simple linear dependence on the square of the cw-drive

and multiphoton effects will be much more important than in QD-driven systems. A detailed study of exciton-driven and cavity-driven systems for the photoluminescence (PL) intensity is presented in Ref. 55.

Summarizing, we find that EID and phonon-induced coupling between the QD and the cavity are two significant effects that are caused by electron-acoustic-phonon scattering in cavity-QED systems. Coherent phonon coupling also causes a temperature-dependent decrease of the effective pump strength and the exciton-cavity coupling rate. All of these phonon-mediated effects depend upon the system Hamiltonian and the properties of the phonon bath spectral function. We also stress that these semiconductor-specific features are quite distinct to the physics of atomic cavity-QED and in general the blind application of an atomiclike ME to these systems will therefore fail. Recently, there has also been several key experimental results on cavity-QED systems that show clearly the effect of phonon bath coupling (e.g., Ref. 19), which further highlight the need for semiconductor quantum optics models to include phonon scattering processes. In this regard, we believe that polaron MEs, such as those presented in this paper, may be very useful for accurately connecting to a wide range of semiconductor cavity-QED experiments in an accurate and straightforward way.

#### Acknowledgments

This work was supported by the National Sciences and Engineering Research Council of Canada and the Canadian Foundation for Innovation.

---

\* Electronic address: chiranjeeb.roy@queensu.ca

† Electronic address: shughes@physics.queensu.ca

<sup>1</sup> Y. Yamamoto and A. Imamoglu, *Mesoscopic quantum optics*, Wiley-Interscience, 2001

<sup>2</sup> U. Hohenester, *Optical properties of semiconductor nanostructures: Decoherence versus Quantum Control* Handbook of Theoretical and Computational Nanotechnology (2006)

<sup>3</sup> D. Press, S. Götzinger, S. Reitzenstein, C. Hofmann, A. Löffler, M. Kamp, A. Forchel, and Y. Yamamoto, *Phys. Rev. Lett.* **98**, 117402 (2007).

<sup>4</sup> N. Akopian, N. H. Lindner, E. Poem, Y. Berlatzky, J. Avron, D. Gershoni, B. D. Gerardot, P. M. Petroff, *Phys. Rev. Lett.* **96**, 130501 (2006)

<sup>5</sup> A. Muller, W. Fang, J. Lawall and G. S. Solomon, *Phys. Rev. Lett.* **103**, 217402 (2009)

<sup>6</sup> R. B. Patel, A. J. Bennett, K. Cooper, P. Atkinson, C. A. Nicoll, D. A. Ritchie and A. J. Shields, *Phys. Rev. Lett.* **100**, 207405 (2008)

<sup>7</sup> see, for example, J. P. Reithmaier, G. Seogonk, A. Löffler, C. Hofmann, S. Kuhn, S. Reitzenstein, L. V. Keldysh, V. D. Kulakovskii, T. L. Reinecke, and A. Forchel, *Nature* **432**, 197 (2004)

<sup>8</sup> T. Yoshie, A. Scherer, J. Hendrickson, G. Khitrova, H. M. Gibbs, G. Rupper, C. Ell, O. B. Shchekin, and D. G. Deppe, *Nature* **432**, 200 (2004).

<sup>9</sup> E. Peter, P. Senellart, D. Martrou, A. Lemaitre, J. Hours, J. M. Gérard, and J. Bloch, *Phys. Rev. Lett.* **95**, 067401 (2005).

<sup>10</sup> A. Imamoglu, H. Schmidt, G. Woods, G. and M. Deutsch, *Phys. Rev. Lett.* **79**, 1467 (1997)

<sup>11</sup> A. N. Vamivakas, C. Y. Lu, C. Matthiesen, Y. Zhao, S. Falt, A. Badolato and M. Atature, *Nature* **467**, 297 (2010)

<sup>12</sup> A. Muller, E. B. Flagg, P. Bianucci, X. Y. Wang, D. G. Deppe, W. Ma, J. Zhang, G. J. Salamo, M. Xiao, and C. K. Shih, *Phys. Rev. Lett.* **99**, 187402 (2007).

<sup>13</sup> E. B. Flagg, A. Muller, J. W. Robertson, S. Founta, D. G. Deppe, M. Xiao, W. Ma, G. J. Salamo and C. K. Shih, *Nature Physics* **5**, 203 (2009).

<sup>14</sup> A. N. Vamivakas, Y. Zhao, C.-Y. Lu and M. Atature, *Nature Physics* **5**, 198 (2009)

<sup>15</sup> S. Ates, S. M. Ulrich, S. Reitzenstein, A. Löffler, A. Forchel, A. and P. Michler, *Phys. Rev. Lett.* **103**, 167402 (2009)

<sup>16</sup> S. Ates, S. M. Ulrich, A. Ulhaq, S. Reitzenstein, A. Löffler, S. Höfling, A. Forchel and P. Michler, *Nature Photonics* **3**,



- 724 (2009)
- <sup>17</sup> A. Majumdar, A. Faraon, E. D. Kim, D. Englund, H. Kim, P. Petroff and J. Vučković, Phys. Rev. B, **82**, 045306 (2010)
  - <sup>18</sup> A. Ulhaq, S. Ates, S. Weiler, S. M. Ulrich, S. Reitzenstein, A. Löffler, S. Höfling, L. Worschech, A. Forchel, and P. Michler, Phys. Rev. B **82**, 045307 (2010)
  - <sup>19</sup> S. M. Ulrich, S. Ates, S. Reitzenstein, A. Löffler, A. Forchel and P. Michler, Phys. Rev. Lett., **106**, 247402 (2011)
  - <sup>20</sup> A. J. Ramsay, T. M. Godden, S. J. Boyle, E. M. Gauger, A. Nazir, B. W. Lovett, A. M. Fox, and M. S. Skolnick, Phys. Rev. Lett. **105**, 177402 (2010)
  - <sup>21</sup> A. J. Ramsay, Achanta Venu Gopal, E. M. Gauger, A. Nazir, B. W. Lovett, A. M. Fox, and M. S. Skolnick, Phys. Rev. Lett. **104**, 017402 (2010)
  - <sup>22</sup> L. Besombes, K. Kheng, L. Marsal and H. Mariette, Phys. Rev. B **63**, 155307 (2001)
  - <sup>23</sup> E. Peter, J. Hours, P. Senellart, A. Vasanelli, A. Cavanna, J. Bloch, and J. M. Gérard, Phys. Rev. B **69**, 041307 (2004).
  - <sup>24</sup> I. Favero, G. Cassaboies, R. Ferreira, D. Darson, C. Voisin, J. Tignon, C. Delalande, G. Bastard, Ph. Roussignol, and J. M. Gérard, Phys. Rev. B **68**, 233301 (2003).
  - <sup>25</sup> D. P. S. McCutcheon and A. Nazir, New J. Phys. **12**, 113042 (2010).
  - <sup>26</sup> D. Mogilevtsev, A. P. Nisovtsev, S. Kilin, S. B. Cavalcanti, H. S. Brandi, and L. E. Oliveira, Phys. Rev. Lett. **100**, 017401 (2008)
  - <sup>27</sup> D. Mogilevtsev, A. P. Nisovtsev, S. Kilin, S. B. Cavalcanti, H. S. Brandi and L. E. Oliveira, J. Phys.: Condens. Matter **21**, 055801 (2009)
  - <sup>28</sup> C. Roy and S. Hughes, Phys. Rev. Lett., **106**, 247403 (2011).
  - <sup>29</sup> A. Majumdar, E. D. Kim, Y. Gong, Yiyang, M. Bajcsy and J. Vučković, Phys. Rev. B, **84**, 085309 (2011).
  - <sup>30</sup> K. Hennessy, A. Badolato, M. Winger, A. A. Imamoglu, Nature **445**, 896 (2007).
  - <sup>31</sup> M. Kaniber, A. Laucht, A. Neumann, J. M. Villas-Boas, M. Bichler, M.-C. Amann, and J. J. Finley, Phys. Rev. B **77**, 161303(R) (2008).
  - <sup>32</sup> R. Oulton, B. D. Jones, S. Lam, A. R. A. Chalcraft, D. Szymanski, D. O'Brien, T. F. Krauss, D. Sanvitto, A. M. Fox, D. M. Whittaker, M. Hopkinson, and M. S. Skolnick, **15** Opt. Express, 17221 (2007).
  - <sup>33</sup> J. Suffczynski, A. Dousse, K. Gauthron, A. Lemaitre, I. Sagnes, L. Lanco, J. Bloch, P. Voisin, and P. Senellart, Phys. Rev. Lett. **103**, 027401 (2009).
  - <sup>34</sup> Y. Ota, S. Iwamoto, N. Kumagai and Y. Arakawa, arXiv:0908.0788 (2009).
  - <sup>35</sup> T. Tawara, H. Kamada, S. Hughes, H. Okamoto, M. Notomi, and T. Sogawa, Opt. Express **17**, 6643 (2009).
  - <sup>36</sup> D. Dalacu, K. Mnyamneh, V. Sazonova, P. J. Poole, G. C. Aers, J. Lapointe, R. Cheriton, A. J. SpringThorpe, and R. L. Williams, Phys. Rev. B **82**, 033301 (2010).
  - <sup>37</sup> M. Calic, P. Gallo, M. Felici, K. A. Atlasov, B. Dwir, A. Rudra, G. Biasiol, L. Sorba, G. Tarel, V. Savona, and E. Kapon Phys. Rev. Lett. **106**, 227402 (2011).
  - <sup>38</sup> J. Xue, K.-D. Zhu and H. Zheng, J. Phys. C **20**, 3252009 (2008).
  - <sup>39</sup> U. Hohenester, A. Laucht, M. Kaniber, N. Hauke, A. Neumann, A. Mohtashami, M. Selinger, M. Bichler, and J. J. Finley, Phys. Rev. B **81**, 201311 (2009).
  - <sup>40</sup> U. Hohenester, Phys. Rev. B **81**, 155303 (2010).
  - <sup>41</sup> P. Kaer, T. R. Nielsen, P. Lodahl, A.-P. Jauho, and J. Mørk, Phys. Rev. Lett. **104**, 157401 (2010).
  - <sup>42</sup> S. Hughes, P. Yao, F. Milde, A. Knorr, D. Dalacu, K. Mnyamneh, V. Sazonova, P. J. Poole, G. C. Aers, J. Lapointe, R. Cheriton and R. L. Williams, Phys. Rev. B **83**, 165313 (2011).
  - <sup>43</sup> G. Tarel and V. Savona, Phys. Rev. B **81**, 075305 (2010).
  - <sup>44</sup> F. Milde, A. Knorr, and S. Hughes, Phys. Rev. B, **78**, 035330 (2008).
  - <sup>45</sup> I. Wilson-Rae and A. Imamoglu, Phys. Rev. B **65**, 235311 (2002)
  - <sup>46</sup> H.-P. Breuer and F. Petruccione, *The Theory of Open Quantum Systems*, Oxford University Press, 2002
  - <sup>47</sup> G. D. Mahan, *Many-Particle Physics*, Plenum, New York, 1990
  - <sup>48</sup> B. Krummheuer, V. M. Axt, and T. Kuhn Phys. Rev. B **65**, 195313 (2002)
  - <sup>49</sup> P. Machnikowski, *Change of Decoherence Scenario and Appearance of Localization due to Reservoir Anharmonicity*, Phys. Rev. Lett. **96**, 140405 (2006).
  - <sup>50</sup> E. A. Muljarov and R. Zimmermann, *Dephasing in Quantum Dots: Quadratic Coupling to Acoustic Phonons*, Phys. Rev. Lett. **93**, 237401 (2004).
  - <sup>51</sup> G. Ortner, D. R. Yakovlev, M. Bayer, S. Rudin, T. L. Reinecke, S. Fafard, Z. Wasilewski, and A. Forchel, *Temperature dependence of the zero-phonon linewidth in InAsGaAs quantum dots*, Phys. Rev. B **70**, 201301(R) (2004).
  - <sup>52</sup> S. Rudin, T. L. Reinecke, and M. Bayer, *Temperature dependence of optical linewidth in single InAs quantum dots*, Phys. Rev. B **74**, 161305(R) (2006).
  - <sup>53</sup> G. Lindwall, A. Wacker, C. Weber, and A. Knorr, *Zero-Phonon Linewidth and Phonon Satellites in the Optical Absorption of Nanowire-Based Quantum Dots*, Phys. Rev. Lett. **99**, 087401 (2007).
  - <sup>54</sup> H. J. Carmichael and D. F. Walls, J. Phys. A: Math. Nucl. Gen. **6**, 1552 (1973)
  - <sup>55</sup> C. Roy and S. Hughes, e-print: arXiv:1109.6530; PRX, in press.
  - <sup>56</sup> H.-P. Breuer, B. Kappler and F. Petruccione, Phys. Rev. A, **59**, 1633 (1999)
  - <sup>57</sup> J. Fischer and H.-P. Breuer, Phys. Rev. A, **76** 052119 (2007)
  - <sup>58</sup> A. Smirne and B. Vacchini, Phys. Rev. A, **82**, 022110 (2010)
  - <sup>59</sup> H. J. Carmichael, *Statistical Methods in Quantum Optics 1: Master Equations and Fokker-Planck Equations*, Springer, 2003
  - <sup>60</sup> M. Scully and M. Zubairy, *Quantum optics*, Cambridge University Press (1997)
  - <sup>61</sup> E. A. Muljarov and R. Zimmermann, Phys. Rev. Lett. **93**, 237401 (2004).
  - <sup>62</sup> S. Rudin, T. L. Reinecke, and M. Bayer, Phys. Rev. B **74**, 161305(R) (2006).
  - <sup>63</sup> P. Borri, W. Langbein, S. Schneider, U. Woggon, R. L. Sellin, D. Ouyang, and D. Bimberg, Phys. Rev. Lett. **87**, 157401 (2001).
  - <sup>64</sup> C. Roy and S. John, Phys. Rev. A, **81**, 023817 (2010)
  - <sup>65</sup> A. Nazir, Phys. Rev. B **78**, 153309 (2008)
  - <sup>66</sup> D. P. S. McCutcheon, N. S. Dattani, E. M. Gauger, B. W. Lovett and A. Nazir,
  - <sup>67</sup> S. M. Tan 1999 J. Opt. B: Quantum Semiclass. Opt. **1**, 424 (1999)
  - <sup>68</sup> A. Ulhaq, S. Ulrich, and P. Michler, *Private communication*.